Ultrasonic melt processing in the low pressure investment casting of Al alloys

J. Barbosa[1*], H. Puga[1]

[1]CMEMS – Center for Microelectromechanical Systems, Universidade do Minho, Azurém

4800-058 Guimarães, Portugal

ABSTRACT

AlSi7Mg investment cast test bars were produced using low-pressure die casting and ultrasonically refined during cooling. The microstructure and mechanical properties of the samples at different distances from the acoustic radiator were characterized for 650ºC pouring temperature. The combined technique lead to cast samples free from gas porosities and solidification defects, promoted the formation of small α-Al globular grains, modified the eutectic silicon, dispersed and decreased the size of intermetallic phases. The alloy mechanical properties were improved, increasing the ultimate tensile strength, yield strength and strain.

Keywords: Aluminum alloys; Investment Casting; Refinement; Ultrasound; Low-pressure

*Corresponding author. Tel: +351253510220/59; Fax: +351253516007

E-mail address: kim@dem.uminho.pt

1. Introduction

Investment casting is a valuable technique to obtain complex small-sized products with high dimensional and geometrical accuracy. However, traditional tilt pouring and turbulent flow promote gas entrapment, oxide formation and erosion of the mould wall which may promote the formation of porosities and inclusions in castings. These problems can be avoided by adapting the low-pressure die casting process to investment casting. According to Campbell (2003), by using pressure differential the melt will rise smoothly into the mould cavity avoiding pickup of dross from the surface and middle regions of the crucible, ensuring high and consistent castings quality avoiding oxide films, inclusions, shrinkage and porosity.

Duse to the intrinsic low cooling rates in ceramic moulds, Al based castings are prone to chemical heterogeneity and microstructure usually consists of coarse dendritic -Al solid solution phase, acicular eutectic silicon and complex intermetallic phases that according to Backerud et al. (1990) may precipitate in the interdendritic and intergranular regions. Garcia-Garcia et al. (2007) found that such microstructure is strongly detrimental to the mechanical behaviour of this alloy, decreasing tensile properties, thus ductility. Chirita et al. (2009) studied the effect of and other microstructure features in the fatigue life of AlSi based alloys and reported that it strongly depends on the SDAS, the amount and morphology of Al-Si eutectic and the presence and morphology of intermetallic phases. Thus, casting defects control and microstructure refinement/modification are imperative to achieve high mechanical performance in Al castings, as reported by Gruzleski et al (1990).

Grain refinement is directly related to the number of active nuclei in the melt. The traditional approach to increase nucleation is by adding master alloys like Al-Ti-B, which release large quantities of $TiAl_3$ and TiB_2 particles in the melt, that are easily enveloped by the α-Al phase during cooling, promoting heterogeneous nucleation. However, chemical refinement presents several drawbacks, namely inability to avoid dendritic structures, no effect over intermetallic

phases besides better distribution and inability to decrease the grain size to values below 200 μm, as demonstrated by Sigworth and Kuhn (2007) and Spittle (2006). Eutectic Si modification is crucial to achieve high mechanical properties, as demonstrated by Garcia-Hinojosa et al. (2003). Gruzleski and Closset (1990) even consider it much more important than grain refinement itself. Na based fluxes are usually used to change Si morphology from acicular to a fine fibrous structure increasing the alloy ductility, as reported by Garcia-Hinojosa et al. (2003), but according to the research and reports of Miresmaeili et al. (2005) and Mcdonald et al. (2004) it may increase the amount of porosities in castings and generate great amount of dross and smoke. An alternative approach to carry out microstructure refinement is ultrasonic vibration. Several models and mechanisms explaining the effect of ultrasonic vibration on grain refinement have been proposed. Eskin (1998) and Abramov (1998) proposed dendrite fragmentation as one of the mechanisms that may induce grain refinement. Liu et al. (2007) and Qian et al. (2009) consider that dendrite fragmentation may occur during ultrasonic vibration, but suggest that cavitation-enhanced heterogeneous nucleation is the most probable mechanism to promote grain refinement. According to Eskin and Eskin (2014), when a liquid metal is submitted to high intensity ultrasonic vibrations, the alternating pressure above the cavitation threshold brings about numerous tiny bubbles in the liquid metal, which start growing, pulsing on a continuous expansion/compression regime and finally collapse. During expansion, bubbles absorb energy in the melt, undercooling the liquid at the bubble-liquid interface, resulting in nucleation on the bubble surface. When bubbles collapse acoustic streaming develops in the melt, distributing the nuclei into the surrounding liquid producing a significant number of nuclei in the molten alloy, thus promoting heterogeneous nucleation. The main objective of this work is to study the capability of the counter gravity pouring technique combined with ultrasonic vibration of the melt during cooling, to eliminate traditional soundness related defects and simultaneously promote the development of ultra refined microstructures.

2. Experimental technique

2.1 Materials

Table 1 presents the chemical composition of the AlSi7Mg alloy used on this work and the equivalent standard alloy.

Table 1 - Chemical composition of the AlSi7Mg0.5 alloy used on this work and the equivalent standard alloy

Alloy	**Chemical composition** (wt %)									**Ref.**
	Si	**Fe**	**Mg**	**Cu**	**Mn**	**Zn**	**Ti**	**Al**	**Res.**	
AlSi7Mg	6.5-7.5	0.6	0.20-0.45	0.25	0.35	0.35	0.25	Bal.	0.15	(1)
Used	7.44	0.2	0.32	0.07	0.07	0.05	0.11	91.53	0.21	(2)

(1) *Aluminum Association, Inc.* (2) Composition of the used alloy obtained by optical emission spectrometry

2.2 Ceramic moulds

The ceramic moulds, with the shape presented in Figure 1 (7) were produced by the traditional investment casting process, using colloidal silica as a binder and SiO_2 grain as stucco to make a shell wall with 7 layers. The mould consisted of a vertical runner and four cylindrical shaped lateral segments with 12 mm in diameter and 120 mm long, which where the cast samples themselves.

2.3 Experimental set-up and procedure

An electrical melting furnace equipped with a SiC crucible of 15 kg capacity was adapted to carry out the low-pressure investment casting process. The melting chamber is fully sealed by a removable top steel plate that also supports the ceramic mould in inverted position. The mould has a top atmospheric riser at the top of the traditional runner, as presented in Figure 1. The plate has a central hole to allow, on a first stage, the introduction of a tubular acoustic radiator to perform melt degassing (Figure 2a) and, on a second stage, the introduction of the ceramic pipe

that allows the liquid metal to rise into the mould (Figure 2b). The ultrasonic device (Fig. 2) used to perform degassing and grain refinement consisted of a novel ultrasonic power supply unit, a high power ultrasonic converter (1200 W) and :

(a) Degassing: 35 mm diameter and 270 mm long acoustic waveguide made of Ti6Al4V and the acoustic load itself, which consists of a 60 mm diameter and 600 mm long Sialon acoustic radiator and the liquid metal.

(b) Refinement: a 35 mm diameter and 270 mm long acoustic waveguide made of Ti6Al4V and the acoustic load itself, which consists on a 20 mm diameter and 90 mm long Ti6Al4V acoustic radiator and the liquid metal.

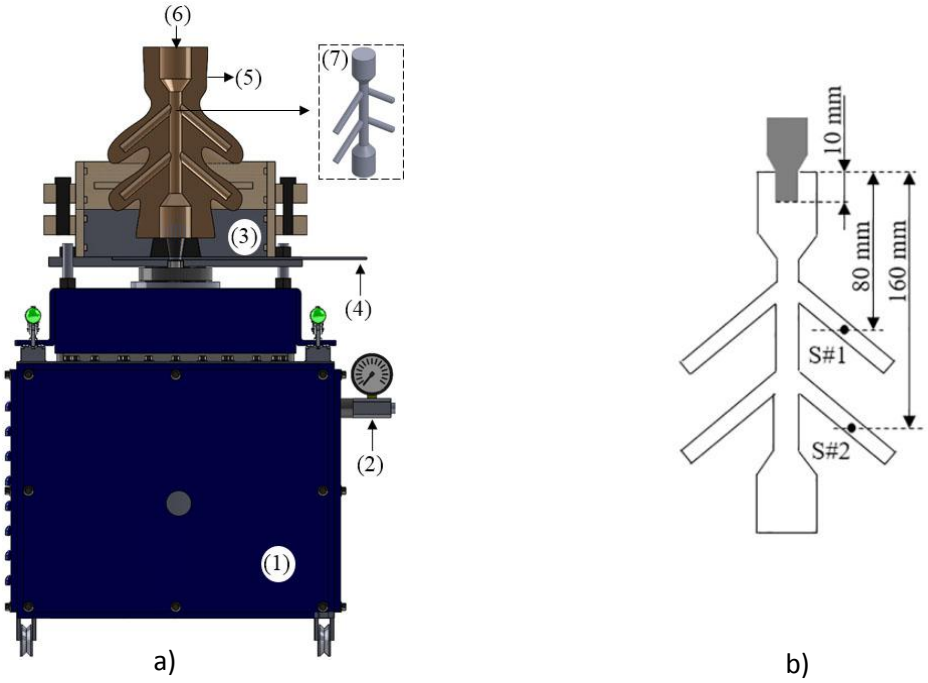

Figure 1 - a) Experimental set-up for the low-pressure investment casting process : (1) Melting chamber; (2) Argon inlet; (3) Moulding box to stand the ceramic shell; (4) Liquid column cutting plate; (5) Ceramic shell; (6) Feeder to insert the refinement acoustic radiator; (7) Wax mould

b) Geometry of the cast samples with indication of the positions S1 and S2, and positioning of the refining ultrasonic radiator at the top of the sprue.

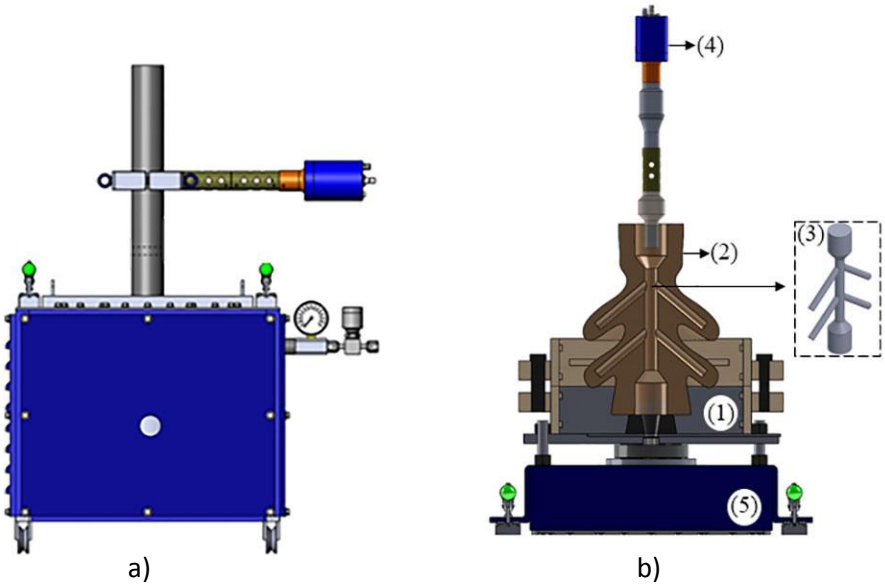

Figure 2 (a) - Experimental set-up for US degassing; (b) Experimental set-up for US refinement: (1) Moulding box to support the ceramic shell; (2) Ceramic shell; (3) Wax mould; (4) US refinement unit; (5) Furnace cover.

The Al7Si0.3Mg alloy was melted at 650ºC and held at that temperature for 30 minutes for homogenization . US degassing vibration was applied for 9 minute, using 20.1±0.1 kHz frequency and 1000W electric power. Reduced Pressure Test (RPT) and the apparent density measurement method were used to evaluate the alloy density before and after 9 minute degassing. Six samples were collected to perform density measurement before and after degassing.

The degassing acoustic radiator was removed, the ceramic mould was positioned over the furnace sealing plate inside a molding box filled with self-set sand. Five ceramic shells were then poured on the conditions described below.

The pressure inside the furnace was then increased over the atmospheric pressure to make the melt rise into the mould cavity, according to the experimental conditions presented in Table 2 and Figure 3. These conditions have been former established by the authors on the aim of previous works, as reported by Puga et al (2016). The pressurization curve was controlled by a

specially designed set of electromagnetic and pneumatic valves using LabView software. Melt temperature was controlled within an accuracy of ±5 ºC.

Table 2. Parameters of the pressure-time (p-t) curves used for mould filling.

Pressure curve	M1 (0 – 5 s)	M2 (5 – 10 s)	M3 (10 – 15 s)	M4 (15– … s)
(1)	600 Pa/s	400 Pa/s	800 Pa/s	0

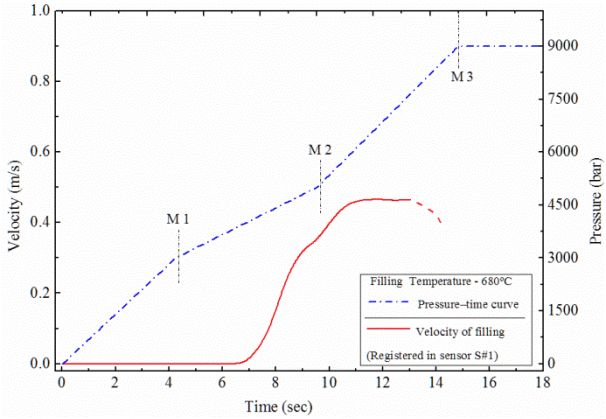

Figure 3 - Average pressure and melt velocity registered in sensor S#1 during cavity filling

After pressure stabilization, the acoustic radiator for melt refinement was deep 10 mm inside the melt through the top feeder of the ceramic mould and ultrasound was supplied to the metal until temperature reached 600ºC at sensor #1, using 19,5±0.4 kHz frequency and 400 W electric power. The casting was then allowed to solidify to room temperature. For the sake of comparison experiments were also carried out without ultrasonic vibration.

2.4 Samples characterization

Samples for microstructure characterization were taken from the vertical sprue by sectioning it perpendicularly to its longitudinal axis at the intersection points between the sprue and the lateral cylinders - around 30 and 120 mm from the radiator. They were ground using 1200 SiC paper

and polished up to 1 μm. Samples for optical microscopy characterization were etched using Keller's reagent to reveal the microstructure. Shape and grain size of constituents were evaluated by optical microscope (OM) with quantitative metallographic analysis capability. Phase identification and chemical composition were evaluated by quantitative EDS analysis using a high resolution FEI Quanta 400 FEG E Scanning Electron Microscope coupled to an EDAX Genesis X4M X-Ray Energy Dispersive Electron Spectrometer. The error associated to elements quantification was 0.2 at%. 10 keV potential and 100 s acquisition time were used for every evaluation. The grain size was evaluated in three 500x400 μm fields using 200x magnification. Each grain was delimited by a contour line using Image Pro Plus software in order to determine its area. Average grain size was then calculated according to ASTM Standard E112-10.

For tensile testing, the specimens were machined from the cylindrical as-cast samples according to EN10002-1(2006). 20 specimens were tested and the results from the upper bars separated from the results of the down bars. Tensile tests were carried out at room temperature and a strain rate of 0.5 mm/min on a INSTRON testing machine - Model 8874, to obtain yield strength, ultimate tensile strength and strain.

3. Results and discussion

3.1 Microstructure of AlSi7Mg0.5 samples without ultrasonic processing

D.G. Eskin and Eskin (2004) suggested that the cavitation is the main mechanism responsible by reduction of hydrogen in melts processed by acoustic energy and the consequent increase of the alloys density. Besides, with decreasing of temperature of melt the viscosity increases and the generation of cavitation is more difficult as been shown by Puga et al. (2009). Thus, according to this evidence, the density steady-state plateaus only was achieved after 9 minutes of degassing and the average value recorded was 2.64±0.02, when compared with an average of density 2.48±0.02 before degassing. Furthermore, for longer degassing times the density tends to

remains constant, and the difference/balance to the theoretical alloy density may be only due to solidification defects.

Fig. 4 (a) and (b) show optical micrographs of the non-ultrasonically refined samples at 30 and 120 mm from the acoustic radiator, respectively. In both cases, the microstructure exhibits fully developed primary α-Al dendrites with branch lengths that in some cases reach 850 μm, with average SDAS of 40±15 μm, as well as the traditional coarse acicular eutectic Si with lamellae that reach 50 μm length. Besides α-Al and silicon plates, SEM analysis revealed the co-existence of other intermetallic phases. According to the chemical composition obtained by EDS (Table 3), those phases seem to be the β-type Al_5FeSi, π-$Al_8Mg_3Si_6Fe$ and Mg_2Si type phases, which is in agreement with reports of Bakerud et al. (1990).

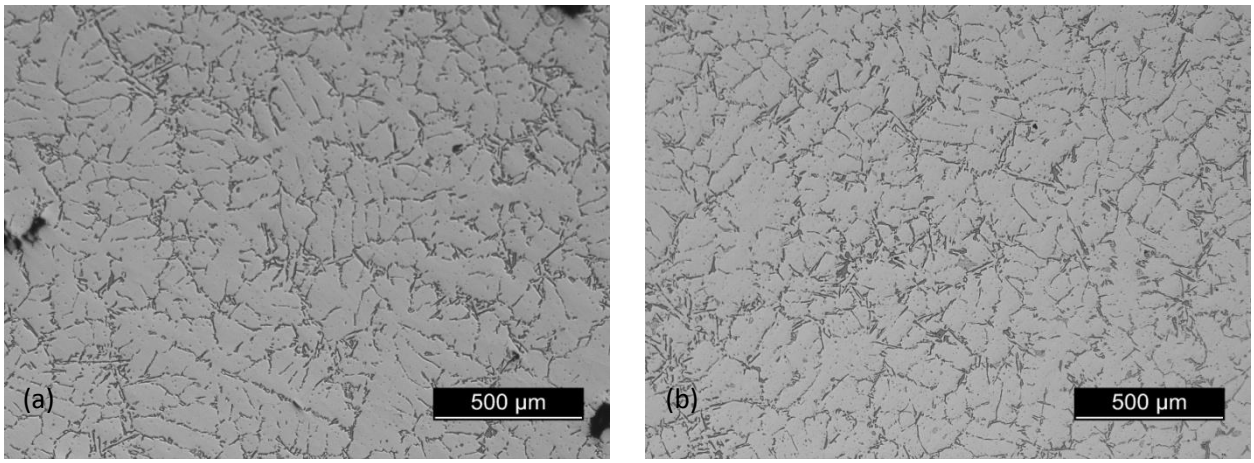

Figure 4 - Microstructure of AlSi7Mg0.5 investment cast samples without ultrasonic treatment at: (a) 30 mm from the acoustic radiator; (b) 120 mm from the acoustic radiator.

Table 3 - Chemical composition of the intermetallic phases present in the as-cast AlSi7Mg0.5 without US treatment.

Zone	**Composition** (% at.)						**Suggested type**
	Mg	**Al**	**Si**	**Mn**	**Fe**	**Cu**	
Z1	0.40	64.74	20.70	<0.20	13.88	<0.20	β-Al_5FeSi
Z2	18.06	49.43	27.29	<0.20	4.57	<0.20	π-$Al_8Mg_3FeSi_6$
Z3	65.67	5.03	29.01	<0.20	<0.20	<0.20	Mg_2Si

Although the melt was ultrasonically degassed the as-cast samples reveal the presence of few porosities in a volume fraction of 1.62±0.8 which is almost constant at both distances from the acoustic radiator. The resultant porosity is mainly due to shrinkage, identified by its irregular shape and interdendritic location. The porosity size is quite heterogeneous, with average area of 240 ±25 μm^2. Round shaped gas porosities have not been detected, confirming the high efficiency of ultrasonic degassing.

3.2 Microstructure of AlSi7Mg0.5 samples with ultrasonic processing

Fig. 5 (a) and (b) present the microstructure of the cast samples submitted to acoustic energy at 30 and 120 mm from the acoustic radiator. At 30 mm from the sonotrode, the microstructure consists of globular α-Al grains with average size of 60 ±5 μm, which changes to a mix of some small rosette like and globular α-Al grains with average size around 110±10 μm at 120 mm from the sonotrode. Moreover, ultrasonic treatment decreased the size of the eutectic lamellae to around 20 ±4 μm at 30 μm from the sonotrode as well as the spacing between lamellae, confirming the reports of Puga et al. (2013) for AlSi9Cu3 alloys, which present the same behavior.

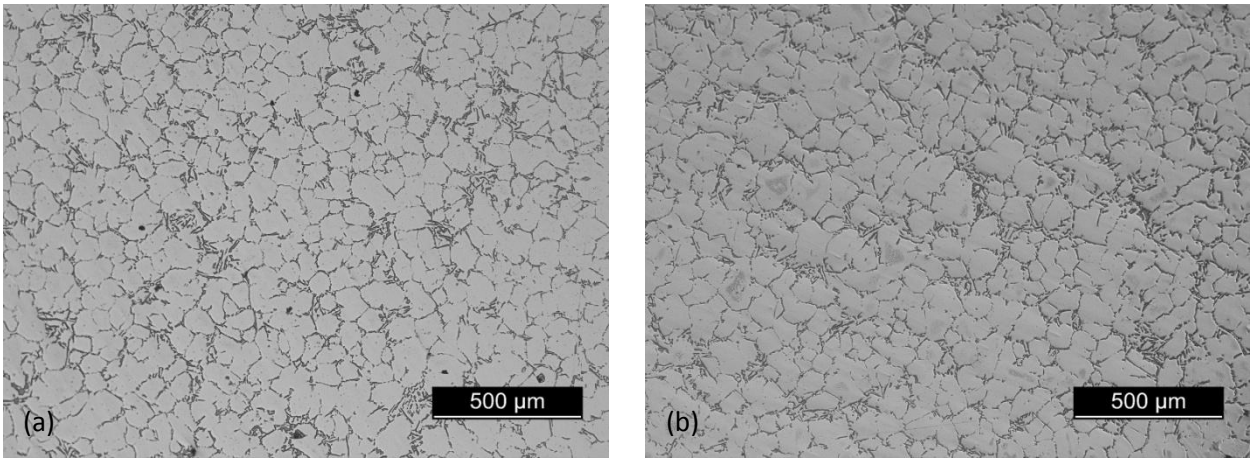

Figure 5 - Microstructure of AlSi7Mg0.5 investment cast samples submitted to ultrasonic treatment at: (a) 30 mm from the acoustic radiator; (b) 120 mm from the acoustic radiator.

These results show that grain refinement tends to be less significant with increasing distance to the acoustic radiator. Not only the grain size tends to increase with increasing distances to the radiator, their circularity also tends to decrease. This can be explained by the decrease of sound pressure at higher distances to the sonotrode, as reported by Eskin (1998). Figure 6 presents the difference in α-Al grain size and length of Si lamellae at different distances to the acoustic radiator in as-cast and ultrasonically processed samples.

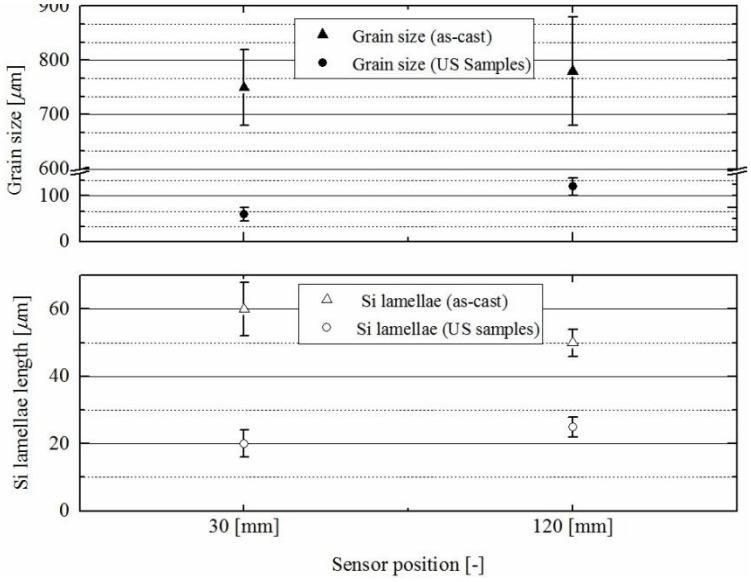

Figure 6 - α-Al grain size and Si lamellae length at 30 and 120 mm from the acoustic radiator in as-cast and US processed samples

SEM characterization suggests the presence of well distributed and extensively refined intermetallic phases that EDS analysis suggest to be α-$Al_{15}(Mn,Fe)_3Si_2$, Mg_2Si and β-Al_5FeSi with branch arms much shorter than those detected in the microstructure of non US treated samples (Table 4). Porosity was almost absent in the analyzed samples, as it can be seen in figs. 5 (a) and (b) and only the presence of extremely scarce gas pores of very low size (less than 5 μm) was detected in 2 samples.

Table 4 - Chemical composition of the intermetallic phases present in the as-cast AlSi7Mg0.5 submitted to ultrasound.

Zone	**Composition** (% at.)						**Suggested type**
	Mg	**Al**	**Si**	**Mn**	**Fe**	**Cu**	
Z1	0.44	68.29	17.07	<0.20	13.72	<0.20	β-Al_5FeSi
Z2	15.06	53.48	25.93	<0.20	5.01	<0.20	π-$Al_8Mg_3FeSi_6$
Z3	64,03	8,31	27,43	<0,20	<0,20	<0,20	Mg_2Si

The β-Al5FeSi phase shows lamellar morphology with average length of 13 ±4μm and appears on a volume fraction of 0.18%, while the π-Al8Mg3FeSi6 phase represents a volume fraction of 0.21%, in the form of polyhedra with about 30 ±2 μm^2 average area and, occasionally, in the lamellar form, reaching 30 μm long. The Mg_2Si phase appears in the form of polyhedra with an average size of 20±2 μm^2 emerging however, occasionally in the form of polyhedra with average area less than 6 μm^2, representing a volume fraction of 0.09%.

Although the refinement of α-Al grains by ultrasound is now quite well understood as referred in section 1, the refinement mechanism of intermetallic phases still needs more research. It is known that intermetallic compounds present in this alloys crystallize at temperatures below 600ºC, as reported by Backerud et al (1990), which is the temperature at which the supply of acoustic energy was stopped. This suggests that the refinement mechanism of intermetallics is not the ultrasonic vibration itself, but the phenomena that occur as a consequence of the ultrasonic vibration. A possible explanation can be attributed to the formation of great number of α-Al globular grains and consequent reduction of the intergranular space, which may have limited the growth of the intermetallic phases, as suggested by Puga et al. (2011) and Kalifa et al. (2010) for other Al-Si based alloys.

Fig. 7 shows the cooling curves obtained for samples without and with US treatment during solidification.

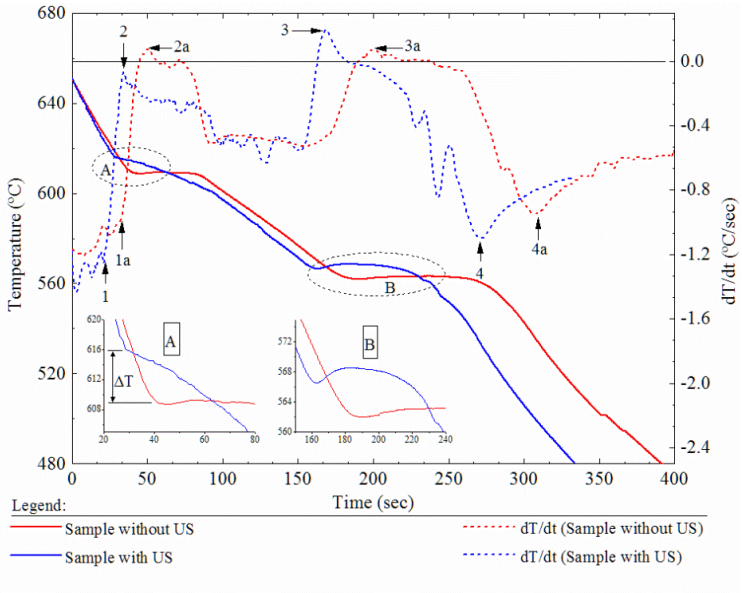

Figure 7 - Cooling curves obtained for samples without and with ultrasonic treatment suggesting the refinement of α-Al (detail A) and eutectic Si phase (detail B).

Precipitation of proeutectic α-Al starts at higher temperature in the sample submitted to US when compared to that solidified without US supply. This is in agreement with the refinement effect on this phase observed by comparing microstructures of Figures 4 and 5. In what concerns to the eutectic reaction of the sample processed by ultrasound, it also starts at higher temperature and has a duration time shorter than that observed for the non US treated sample. The differences detected in solidification curves and the resultant microstructures, clearly suggest that US supply worked as germinator of solidification nuclei both on the beginning of proeutectic precipitation (detail A) and the beginning of the eutectic reaction (detail B), revealing its effect in the refinement of *a*-Al grains and and eutetic Si lamellae.

3.3 Mechanical properties

Fig. 8 presents the mechanical properties obtained for samples with and without ultrasonic treatment at different distances from the acoustic radiator. The ultrasonic treatment clearly

improved the alloy mechanical properties, especially in what concerns to ductility. It is evident that the ultimate tensile strength, yield strength and elongation increased significantly with ultrasonic processing.

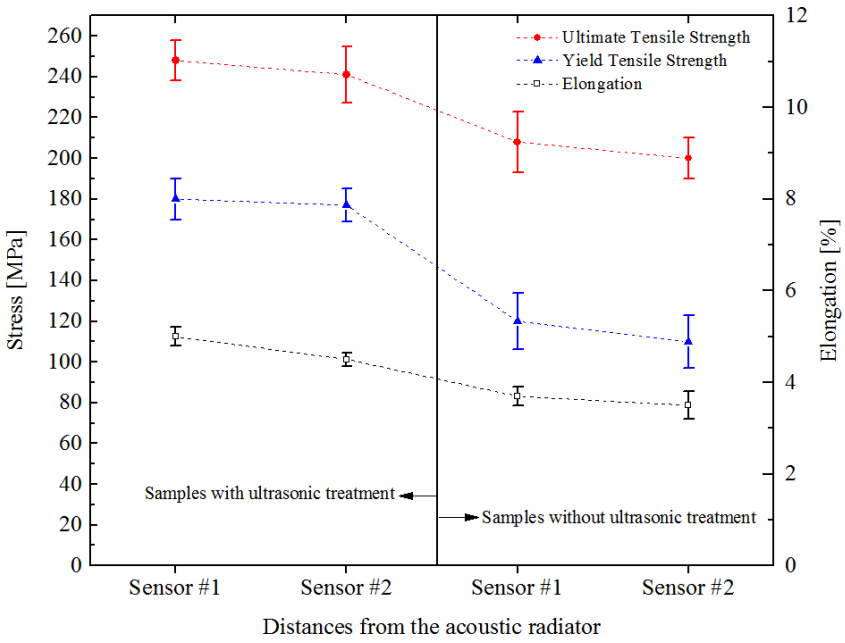

Figure 8 - Ultimate Tensile Strength, Yield Strength and elongation at different distances from the sonotrode, in as-cast and ultrasonic treated AlSi7Mg samples

It is well known that mechanical properties of Al-Si alloys depend on several factors, with particular emphasis to the microstructure morphology and the presence of Fe-rich intermetallic compounds, as reported by Garcia-Garcia et al (2007) and Ceschini et al (2009). Ammar et al. (2008) and Teng et al. (2009) reported that the presence of porosities and their size and distribution are also highly detrimental to the mechanical properties of Al based alloys. Moreover, the morphology of eutectic silicon is determinant to the mechanical properties, as demonstrated by Garcia-Hinojosa et al. (2003) and Gruzleski and Closset (1990). Although, the size and morphology of the primary aluminum phase also play a significant role in the alloy mechanical behavior , as reported by Sigworth and Kuhn (2007) and Spittle (2006). Moreover, in the particular case of Al-Si-Mg alloys, Li et al. (2004)(1) reported that the sharp ends of the brittle β-Al_5FeSi acicular phase can act as stress concentrators, decreasing ductility.

Taking into consideration the above mentioned, the UTS increase verified in our research can be attributed to the combined effect of the globular shape and small size of the α-Al grain, the reduction of the volume fraction of β-Al_5FeSi, the fine and short eutectic silicon fibers and the elimination of porosities.

Since both processing routes included the same degassing process, it is expected that the level of microporosity due to the presence of hydrogen is similar in every sample, which can be confirmed by comparing figures 4 and 5. Thus, the grain size and morphology are the main contributors to the performance of the bulk material in terms of mechanical properties, confirming findings of Eskin and Eskin (2014) and Puga et al.(2011).

4. Conclusions

The main conclusions can be drawn from the developed study:

- The developed technique (low-pressure pouring combined with ultrasonic refinement of the cast alloy directly in the ceramic mould) proved to be an extremely efficient way to obtain high integrity Al-Si based castings, free from porosities and with fully refined microstructure;
- Ultrasonic processing not only avoids/decreases the development of gas porosities but also leads to a significant decrease in solidification defects like shrinkage;
- Direct ultrasonic processing fully refines microstructure, leading to the formation of α-Al globular grains, fibrous eutectic silicon phase and well dispersed intermetallic phases with small dimensions;
- The combined technique promotes the increase of mechanical properties, namely ultimate tensile strength, yield strength and elongation to failure.

Acknowledgements

This work is supported by FCT with the reference project UID/EEA/04436/2013, by FEDER funds through the COMPETE 2020 - Programa Operacional Competitividade e Internacionalização (POCI) with the reference project POCI-01-0145-FEDER-006941. Also this work has been supported by the Post-Doctoral grant SFRH/BPD/76680/2011.

References

Abramov, O.V., 1998. High-Intensity Ultrasonics Theory and Industrial Applications, first edition. Gordon and Breach Science Publishers, Amsterdam.

Ammar, H.R., Samuel, A.M., Samuel, F.H., 2008. Effect of casting imperfections on the fatigue life of 319-F and A356-T6 Al-Si casting alloys. Materials Science and Engineering A 473, 65-75.

Backerud, L., Chai, G., Tamminen, J., 1990. Solidification Characteristics of Aluminum Alloys. Vol. 2: Foundry Alloys. AFS/Skanaluminium, Stokholm.

Campbell J., 2003. Castings, 2th Ed., Butterworth-Heinemann, Oxford, United Kingdom.

Ceschini L., Buromei, I., Morri, A., Seifeddine, S., Svensson, I., 2009. Microstructure, tensile and fatigue properties of the Al–10%Si–2%Cu alloy with different Fe and Mn content cast under controlled conditions. Journal of Materials Processing Technology 209, 5669-5679.

Chirita, G., Stefanescu, I., barbosa, J., Puga, H., Soarers, D., Silva, F.S., 2009. On assessment of processing variables in vertical centrifugal casting technique. International Journal of Cast Metals Research, 22(5), 382-389.

Eskin, G.I., 1998. Ultrasonic Treatment of Light Alloy Melts, first edition. Gordon and Breach Science Publishers, Amsterdam.

Eskin, G.I., Eskin, D.G., 2014. Ultrasonic treatment of light alloy melt, CRC Press, Boca Raton.

Garcia-Garcia, G., Espinoza-Cuadra, J., Mancha-Molinar, H., 2007. Copper content and cooling rate effects over second phase particles behavior in industrial aluminum-silicon alloy 319. Materials & Design 28, 428-433.

García-Hinojosa, J.A., González, C.R., González, G.M., Houbaert, Y., 2003. Structure and properties of Al-7Si-Ni and Al-7Si-Cu cast alloys non-modified and modified with Sr. Journal of Materials Processing Technology 143-144, 306-310.

Gruzleski, J.E., Closset, B.M., 1990. The Treatment of liquid Aluminum-Silicon Alloys American Foundryman Society, Des Plaines, IL, USA.

Khalifa, W., Tsunekawa, Y., Okumiya, M., 2010. Effect of ultrasonic treatment on the Fe-intermetallic phases in ADC12 die cast alloy. Journal of Materials Processing Technology 210, 2178-2187.

Li, Z., Samuel, A.M., Samuel, F.H., Ravindran, C., Valtierra, S., Doty, H.W., 2004(1). Parameters controlling the performance of AA319-type alloys: Part I. Tensile properties. Materials Science and Engineering A 367, 96-110.

Liu, Q.M., Zhai, Q.J., Qi, F.P., Zhang, Y., 2007. Effects of power ultrasonic treatment on microstructure and mechanical properties of T10 steel. Materials Letters **61**(11-12), 2422-2425.

Mcdonald, S.D., Dahle, A.K., Taylor, J.A., StJohn, D.H., 2004. Modification-related porosity formation in hypoeutectic aluminum-silicon alloys. Metallurgical and Materials Transactions B 35B, 1097-1106.

Miresmaeili, S.M., Campbell, J., Shabestari, S.G., Boutorabi, S.M.A., 2005. Precipitation of Sr-rich intermetallic particles and their influence on pore formation in Sr-modified A356 alloy. Metallurgical and Materials Transactions A 36A, 2342-2349.

Sigworth, G.K., Kuhn, T.A., 2007. Grain Refinement of Aluminum Casting Alloys AFS Transactions 67(2), 1-12.

Spittle, J.A., 2006. Grain refinement in shape casting of aluminium alloys. International Journal of Cast Metals Research 19, 210-222.

Teng, X., Mae, H., Bai, Y., Wierzbicki, T., 2009. Pore size and fracture ductility of aluminum low pressure die casting. Engineering Fracture Mechanics 76, 983-996.

Puga, H., Barbosa, J., Soares, D., Silva, F., Ribeiro, S., 2009. Recycling of aluminium swarf by direct incorporation in aluminium melts. Journal of Materials Processing Technology 209, 5195-5203.

Puga, H., Costa, S., Barbosa, J., Ribeiro, S., Prokic, M., 2011. Influence of ultrasonic melt treatment on microstructure and mechanical properties of AlSi9Cu3 alloy. Journal of Materials Processing Technology 211, 1729-1735.

Puga, H., Barbosa, J., Costa, S., Ribeiro, S., Pinto, A.M.P., Prokic, M., 2013. Influence of indirect ultrasonic vibration on the microstructure and mechanical behaviour of Al-Si-Cu alloy. Materials Science and Engineering A 560, 589-595.

Puga, H., Barbosa, J., Azevedo, T., Alves, J.L., 2016. Low pressure sand casting of ultrasonically degassed Al7SiMg alloy: Modelling and experimental validation of mould filling. Materials and Design 94, 384-391.

Qian, M., Ramirez, A., Das, A., 2009. Ultrasonic refinement of magnesium by cavitation: Clarifying the role of wall crystals. Journal of Crystal Growth 311, 3708-3715.

Figure Caption

Figure 1 (a) - Experimental set-up for the low-pressure investment casting process : (1) Melting chamber; (2) Argon inlet; (3) Moulding box to stand the ceramic shell; (4) Liquid column cutting plate; (5) Ceramic shell; (6) Feeder to insert the refinement acoustic radiator; (7) Wax mould

(b) - Geometry of the cast samples with indication of the positions S1 and S2, and positioning of the refining ultrasonic radiator at the top of the sprue.

Figure 2 (a) - Experimental set-up for US degassing; (b) Experimental set-up for US refinement: (1) Moulding box to stand the ceramic shell; (2) Ceramic shell; (3) Wax mould; (4) US refinement unit; (5) Furnace cover.

Figure 3 - Average pressure and melt velocity registered in sensor S#1 during cavity filling

Figure 4 - Microstructure of AlSi7Mg0,5 investment cast samples without ultrasonic treatment at: (a) 30 mm from the acoustic radiator; (b) 120 mm from the acoustic radiator.

Figure 5 - Microstructure of AlSi7Mg0,5 investment cast samples submitted to ultrasonic treatment at: (a) 30 mm from the acoustic radiator; (b) 120 mm from the acoustic radiator.

Figure 6 - α-Al grain size and Si lamellae length at 30 and 120 mm from the acoustic radiator in as-cast and US processed samples

Figure 7 - Cooling curves obtained for samples without and with ultrasonic treatment suggesting the refinement of α-Al (detail A) and eutectic Si phase (detail B).

Figure 8 - Ultimate Tensile Strength, Yield Strength and elongation at different distances from the sonotrode, in as-cast and ultrasonic treated AlSi7Mg samples

Table Caption

Table 1 - Chemical composition of the AlSi7Mg0,5 alloy used on this work and the equivalent

Table 2. Parameters of the pressure-time (p-t) curves used for mould filling.

Table 3 - Chemical composition of the intermetallic phases present in the as-cast AlSi7Mg0,5 without US treatment.

Table 4 - Chemical composition of the intermetallic phases present in the as-cast AlSi7Mg0,5 submitted to ultrasound.